Hindawi Publishing Corporation
International Journal of Photoenergy
Volume 2012, Article ID 906198, 7 pages
doi:10.1155/2012/906198

Research Article

Influence of TiO_2 Nanocrystals Fabricating Dye-Sensitized Solar Cell on the Absorption Spectra of N719 Sensitizer

Puhong Wen, Yinfeng Han, and Weixing Zhao

Department of Chemistry and Chemical Engineering, Baoji University of Arts and Science, 1 Gaoxin Road, Shaanxi, Baoji 721013, China

Correspondence should be addressed to Puhong Wen, wenpuhong@gmail.com

Received 9 April 2012; Accepted 22 May 2012

Academic Editor: Mohamed Sabry Abdel-Mottaleb

Copyright © 2012 Puhong Wen et al. This is an open access article distributed under the Creative Commons Attribution License, which permits unrestricted use, distribution, and reproduction in any medium, provided the original work is properly cited.

The absorption spectra of N719 sensitizer anchored on the films prepared by TiO_2 nanocrystals with different morphology and size were investigated for improving the performance of dye-sensitized solar cell (DSC). We find that the morphology and size of TiO_2 nanocrystals can affect the UV-vis and FT-IR spectra of the sensitizer anchored on their surfaces. In particular, the low-energy metal-to-ligand charge-transfer transitions (MLCT) band in the visible absorption spectra of N719 is strongly affected, and locations of these MLCT bands revealed larger differences. The results indicate that there is a red shift of MLCT band in the spectra obtained by using TiO_2 nanocrystals with long morphology and large size compared to that in solution. And it produced a larger red-shift on the MLCT band after TiO_2 nanocrystals with small size mixed with some long nanocrystals. Accordingly, the utilization rate to visible light is increased. This is a reason why the DSC prepared by using such film as a photoelectrode has better performance than before mixing.

1. Introduction

As such a concept for photovoltaic devices, dye-sensitized solar cells (DSCs) have received considerable attention since 1991 due to their relatively high efficiency and low fabrication cost [1–6]. Ruthenium polypyridyl complexes are commonly used as dyes in DSCs, and the highest power conversion efficiency of 11.3% has been achieved [7]. The typical DSC consists of a dye-coated mesoporous TiO_2 nanoparticle film sandwiched between two transparent electrodes, and a liquid electrolyte, traditionally containing the tri-iodide/iodide redox couple, fills the pores of the film and contacts the nanoparticle. Many factors, in particular, in the part of the photoelectrode such as morphology, particle size, and crystal structure of semiconductor TiO_2 [8], can affect the performance of DSC. They should be investigated in order to raise power conversion efficacy. In the past decade, much work has been done to improve the photovoltaic parameters of DSC including optimizing nanostructured semiconductor electrodes [9, 10], sensitizers [11, 12], redox electrolytes [13, 14], and electric additives [15–17]. Only few studies, however, focused on the effect of the TiO_2 nanocrystals on the absorption spectra of the sensitizer anchored on their surfaces. Nazeeruddin et al. [18] reported merely the differences in the absorption spectra of sensitizer N3, N719, and N712 anchored on TiO_2 nanocrystals. In this study, the absorption spectra of sensitizer N719 anchored on TiO_2 nanocrystals with different morphology and particle size were investigated for increasing the utilization rate to visible light. The result is helpful to improve the performances of DSCs.

2. Experimental Details

2.1. Materials. 10 wt% tetrabutylammonium hydroxide (TBAOH) aqueous solution and *n*-propylamine (PA) solution were purchased from Tokyo chemicals. N719 (*cis*-di(thiocyanate)bis(2,2′-bipyridyl-4,4′-dicarboxylate)-ruthenium(II) bis-tetrabutyl-ammonium) was purchased from Sigma-Aldrich. ST01 (commercial TiO_2 powder) was obtained from Ishihara. ST111 (commercial TiO_2 powder) was obtained from Titan Kogyo. Other chemicals and reagents were of analytical grade, and all the reagents were used as received without further purification.

2.2. Synthesis of TiO_2 Nanocrystals. To prepare anatase samples QTBA, QPA, and LPA, an H^+-form-layered titanate ($H_{1.07}Ti_{1.73}O_4$) with lepidocrocite-like structure was treated in a TBAOH solution or a PA solution to exfoliate the layered titanate into its nanosheets. The titanate nanosheet solution was then reacted under hydrothermal conditions [19, 20]. The QTBA was obtained by hydrothermal reaction of a titanate nanosheet solution of TBAOH at 120°C and pH 1.8. The samples QPA and LPA were obtained by hydrothermal reaction of a titanate nanosheet solution of PA at 120°C and pH 1.9, and at 135°C and pH 11.3, respectively.

2.3. Fabrication of Dye-Sensitized Solar Cell. A TiO_2 film electrode was prepared by the doctor-blade technique, using TiO_2 nanocrystal paste on an FTO glass plate (25 × 25 mm). The paste sample was prepared by dispersing TiO_2 nanocrystals sample in a 0.2 mol/L HNO_3 solution containing 3 wt% of Triton X-100, 5 wt% of acetylacetone, and 10 wt% of polyethylene glycol (PEG) (molecular weight of 20, 000). The TiO_2 content in the paste was adjusted to about 15–18 wt% to control the thickness of the TiO_2 film. After being coated with the paste on the FTO glass plate, the TiO_2 film electrode was calcined at 450°C for 30 min and then immersed into a 3×10^{-4} mol/L N719 dye solution in a mixed solvent of acetonitrile and *tert*-butyl alcohol (1 : 1 volume ratio) for 24 h to adsorb the dye onto the TiO_2 electrode. The DSC was comprised of the dye-adsorbed TiO_2 electrode and a Pt-coated conducting glass counter-electrode, with an electrolyte solution between the electrodes. The electrolyte solution contained butylmethylimidazolium iodide (0.60 mol/L), I_2 (0.03 mol/L), guanidinium thiocyanate (0.10 mol/L), and 4-*tert*-butylpyridine (0.50 mol/L) in a mixed solvent of acetonitrile and valeronitrile (85% : 15% volume ratio).

2.4. Photovoltaic Measurements. The photocurrent-voltage characteristic curves for the DSCs were measured using a Hokuto-Denko BAS100B electrochemical analyzer under irradiation with simulated sunlight of AM 1.5 (100 mW/cm^2), using a sunlight simulator (YSS-E40, Yamashita Denso) and a 0.25 cm^2 mask. The thicknesses of the TiO_2 films were measured using a SURFCOM 480A surface-shape determiner.

2.5. Physical Analysis. Powder X-ray diffraction (XRD) analysis of the samples was carried out on a SHIMADZU XRD-6100 X-ray diffractometer with Cu Kα (λ = 0.15418 nm) radiation for the investigation of the crystal structure of the samples. The size and morphology of the particles were observed using fieldemission scanning electron microscopy (FE-SEM) (Hitachi, Model S-900). Transmission electron microscopy (TEM) observation and selected-area electron diffraction (SAED) were performed on a JEOL Model JEM-3010 system at 300 kV, and the powder sample was supported on a microgrid. Nitrogen gas adsorption was carried out on a Quantachrome Autosorb-1-MP apparatus. The specific surface area was calculated from the adsorption data using the Brunauer-Emmett-Teller (BET) method. FT-IR spectra of the samples were measured on a Perkin Elmer Spectrum One spectrophotometer at a resolution of better than 2 cm^{-1} using the KBr technique. UV-visible spectra were recorded on a SHIMADZU UV-2450 spectrophotometer. A corresponding blank TiO_2 film was used as reference to obtain the UV-visible spectrum of the dye adsorbed on the TiO_2 film. Both have the same thickness.

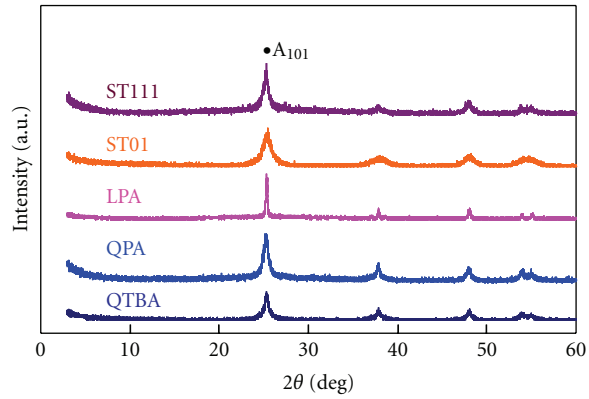

Figure 1: XRD patterns of the self-prepared (QTBA, QPA, and LPA) and the commercial (ST01 and ST111) TiO_2 nanocrystal samples. These samples are single phase of anatase. The width of diffraction peaks indicates the crystallinity increasing order of ST01 < ST111 < QTBA < QPA < LPA.

3. Results and Discussion

3.1. Characterizations of TiO_2 Nanocrystals. To investigate the influences of the morphology and size of TiO_2 nanocrystalstals on the UV-vis and FT-IR spectra of the sensitizer anchored on their surfaces, five kinds of TiO_2 nanocrystal samples with different crystal sizes and crystal morphologies were used in this study. Two are typical commercial TiO_2 nanocrystal samples, ST01 and ST111, with different crystal sizes. And the rest are three self-prepared anatase nanocrystal samples with different crystal morphologies and sizes: QTBA, QPA, and LPA. They were prepared from exfoliated layered titanate ($H_{1.07}Ti_{1.73}O_4$) nanosheet solutions by hydrothermal reactions [19–21]. An XRD study indicated that they are single phase of anatase as shown in Figure 1. The width and acutance of diffraction peaks indicate the crystallinity increasing order of ST01 < ST111 < QTBA < QPA < LPA.

The TEM images of these TiO_2 nanocrystals are presented in Figure 2. The QTBA and QPA samples have quadrate crystal morphologies, but the size of the later is as large again as QTBA size of about 20 nm in width. The LPA sample has long nanoleaf-like crystal morphologies and larger size of about 30 nm in width and 300 nm in length. The SAED result indicated that QPA is a single crystal of anatase phase, which agrees with the XRD result in Figure 1.

The change in morphology can be explained by the effect of pH value on the dissolution reaction in the synthesis process [19]. The dissolution reactions along the (100), (001), and (101) planes of anatase phase can occur and cut the sheetlike particles into the quadrate anatase nanocrystals because of the acidic conditions (pH < 2) in the synthesis

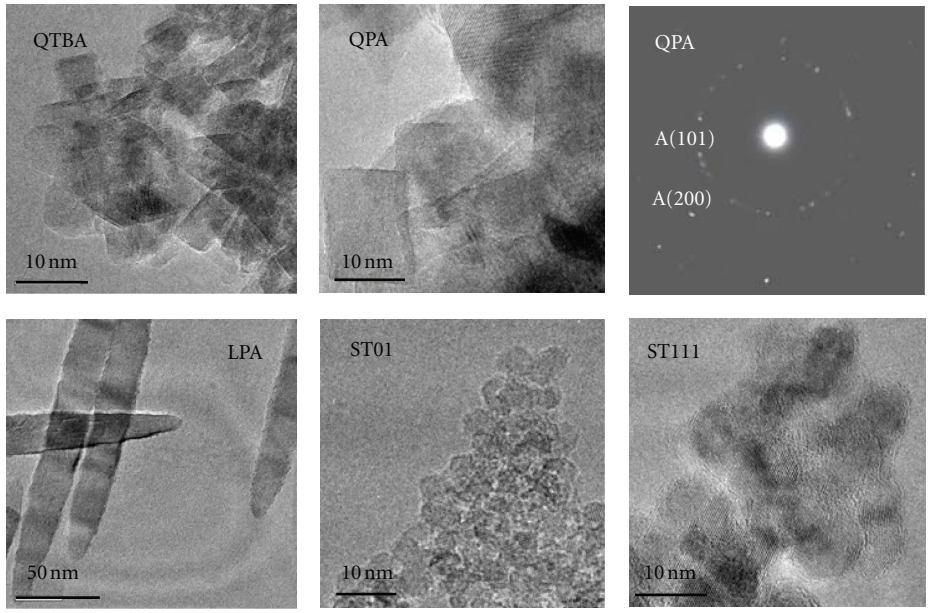

Figure 2: TEM images of the self-prepared (QTBA, QPA, and LPA) and the commercial (ST01 and ST111) TiO_2 nanocrystal samples and the SAED patterns of QPA sample.

Table 1: Morphology and surface area of the TiO_2 nanocrystals and the optical data of the N719 dye adsorbed onto TiO_2 nanocrystals films.

Sample	Morphology	S_{BET} (m^2/g)	UV-vis abs. λ_{max} (nm)[b]		FT-IR vibration band wavenumber (cm^{-1})[c]
			MLCT	π-π^*	
ST01	Spherical	349	398sh 523		2105m 1657vs 1608vs 1541m 1467w 1430w 1403w 1373vs 1262vw 1235w 1165w 1107vw
ST111	Spherical	312	398sh 537		2105s 1657vs 1608vs 1542m 1466vw 1429m 1402w 1372vs 1261vw 1236w 1166m 1109vw
QTBA	Quadrate	131	395sh		2103w 1657vs 1607vs 1540m 1467w 1429w 1402w 1372vs 1262vw 1236w 1167w 1108vw
QPA	Quadrate	66	536		2104w 1713vw 1614vs 1544m 1466vw 1430m 1403m 1384vs 1262w 1231vw 1112w
LPA	Leaflike	35	598		2925s 2855m 2343w 2104m 1741m 1619s 1542m 1466w 1436w 1402m 1379s 1234m 1165w 1108w
QTBA-LPA			631		
QPA-LPA			571		
N719[a]			390 531	215 253sh 313	2964s 2876w 2104vs 1714s 1611s 1543m 1467m 1437vw 1406m 1370s 1237s 1149vw 1021w

[a] UV-vis absorption measured in ethanol, [b] sh: shoulder, [c] vs: very strong; s: strong; m: medium; w: weak; vw: very weak.

processes of QTBA and QPA samples, and the dissolution reaction only along the (100) plane can occur and cut the sheetlike particles into long nanoleaf-like anatase nanocrystals because the value of pH is 11.3 in the synthesis process of LPA sample. The ST01 and ST111 samples have spherical crystal morphologies with sizes of about 7 nm (ST01) and 10 nm (ST111), respectively. Figure 3 shows FE-SEM images of the single crystal of QTBA and LPA and the films prepared by using the corresponding single crystal. The results agree with TEM analysis and further indicate that the single crystals of QTBA and LPA are flat particles. The BET (Brunauer-Emmett-Teller) specific surface areas (S_{BET}) of the TiO_2 nanoparticles samples are shown in Table 1. The S_{BET} values increase in the order of LPA < QPA < QTBA < ST111 < ST01, which are in agreement with their crystal sizes.

3.2. Absorption Spectra Properties. The UV-vis and FT-IR absorption spectra properties of the N719 sensitizer anchored on the surfaces of TiO_2 nanocrystals ST01, ST111, QTBA, QPA, and LPA samples are shown in Table 1. The data about UV-vis absorption spectra of the N719 sample in ethanol solution and FT-IR absorption spectra of solid N719 sample are given in Table 1 for the comparison. The UV-vis absorption spectra of the N719 sample in ethanol

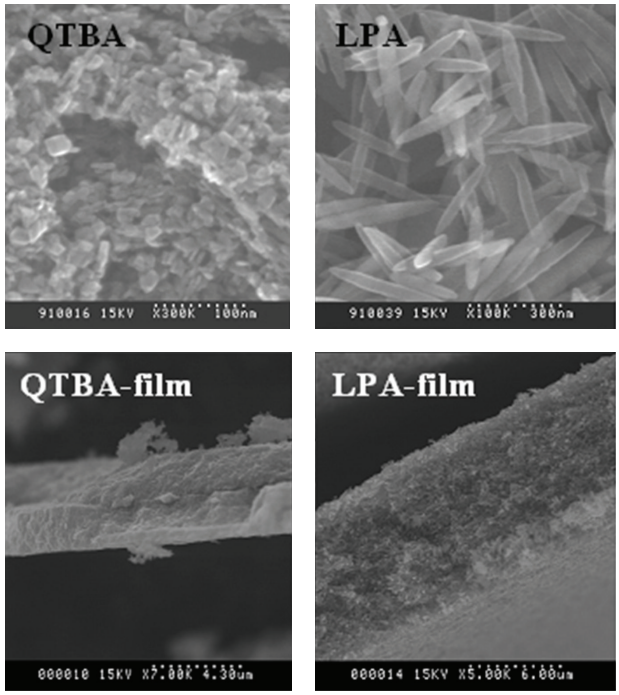

Figure 3: FE-SEM images of anatase TiO_2 nanocrystals QTBA and LPA samples and the films prepared by QTBA and LPA samples.

solution reveals four broad bands as shown in Figure 4(a). The two broad visible bands at 531 and 390 nm are assigned to metal-to-ligand charge-transfer (MLCT) origin. The bands in the UV region at 313 and 215 nm with a shoulder at 253 nm are specified to intraligand (π-π^*) charge-transfer transitions. Figure 4(b) shows a comparison of the absorption spectra of N719 dye adsorbed onto the films (6 to 10 μm thick) prepared by TiO_2 nanocrystals samples with different morphologies and sizes, and UV-vis absorption spectra of corresponding blank films without absorption band in the visible region are shown in Figure 4(c) for comparison. The low-energy MLCT maximum in N719 dye is considerably shifted upon adsorption onto these films compared to the solution spectra. The blue shifts of the low-energy MLCT band occur onto ST01 (8 nm) and QTBA (14 nm) films. On the other hand, the red shifts of the low-energy MLCT band occur to LPA (67 nm), ST111 (6 nm), and QPA (5 nm) films, and the film prepared by mixing QTBA (80%) and LPA (20%), which induces the largest red shift from 531 to 631 nm. The results reveal that there is a red shift of MLCT band in the spectra obtained by using TiO_2 nanocrystals with long morphology and large size compared to that in solution. And a larger red shift occurs on the MLCT band after TiO_2 nanocrystals with small size mixed with some long nanocrystals. Accordingly, it increases the utilization rate to visible light. The results indicate that the morphology and size of TiO_2 nanocrystals can lead to a shift in the low-energy MLCT of N719 dye. The shift is due to the change in the energy of the lowest unoccupied molecular orbital (LUMO) of the ligand, causing the π-π^* and dπ-π^* transitions to occur at higher or lower energies [18].

The data about the FT-IR absorption spectra of solid N719 sample in Table 1 show the characteristic band at 2104 cm^{-1} due to the ν(NCS) group. The bands at 1714 and 1237 cm^{-1} are assigned to the ν(C=O), and ν(C–O) groups, respectively. The other two strong bands at 1611 ($-COO^-_{as}$) and 1370 ($-COO^-_{s}$) cm^{-1} are assigned to the asymmetric and the symmetric stretch of the carboxylate group, respectively. The bands at 1611, 1543, and 1406 cm^{-1} are assigned to the bipyridyl ν(C=C) absorption. The band at 1467 cm^{-1} is assigned to the $\delta(CH_2)$ of the Bu_4N^+ cations. The bands at 2876 and 2964 cm^{-1} are assigned to ν(C–H) of tetrabutylammonium symmetric and asymmetric $-CH_2$ and $-CH_3$ groups, respectively [22]. To achieve high quantum yields of the excited state electron transfer process, the dye ideally needs to be in intimate contact with the semiconductor surface. The carboxylate functional groups of the dye serve as grafting agents for the oxide surface of the TiO_2 films. It is an important feature in a dye-sensitized solar cell for electronic communication between the complex and the substrate. The ruthenium complex N719 contains two carboxylic acid and two carboxylate groups. Thus, it can anchor onto the TiO_2 surface by a close overlap of the ligand π^* orbitals and the titanium 3D orbitals. A comparison of FT-IR absorption spectra properties of N719 sensitizer anchored on the surfaces of the TiO_2 nanocrystals ST01, ST111, QTBA, QPA, and LPA samples is shown in Figure 5. The major difference between the solid and the adsorbed N719 spectra occurs in carboxylic acid and carboxylate group bands. The $\nu(-COO^-_{s})$ bands in all adsorbed N719 samples are shifted to higher energy compared to the carboxylate group band (1370 cm^{-1}) of N719 complex. The shifts increase in the order of ST111 = QTBA (2 cm^{-1}) < ST01 (3 cm^{-1}) < LPA (9 cm^{-1}) < QPA (14 cm^{-1}). The $\nu(-COO^-_{as})$ band at 1611 cm^{-1} also occurs in the shifts, which is to lower energy for ST01 (3 cm^{-1}), ST111 (3 cm^{-1}) and QTBA (4 cm^{-1}), but higher energy for QPA (3 cm^{-1}) and LPA (8 cm^{-1}). The ν(C–O) bands in all adsorbed N719 samples are shifted to lower energy compared to that (1237 cm^{-1}) in N719 complex. The increasing shift order of ST111 = QTBA (1 cm^{-1}) < ST01 (2 cm^{-1}) < LPA (3 cm^{-1}) < QPA (6 cm^{-1}) agrees with that of the $\nu(-COO^-_{s})$ bands. The ν(C=O) band is shifted to lower energy by 57 cm^{-1}, from 1714 to 1657 cm^{-1} for ST01, ST111, and QTBA, and that in QPA is shifted only 1 cm^{-1}, but the band in LPA is at 1741 cm^{-1} shifting to higher energy (27 cm^{-1}). The ν(NCS) group, the bipyridyl ν(C=C) at 1543 and 1406 cm^{-1}, and the $\delta(CH_2)$ of the Bu_4N^+ cations bands are shifted hardly with the change of the morphology and the size of TiO_2 nanocrystals. The results indicated that the morphology and size of TiO_2 nanocrystals strongly affect on the $\nu(-COO^-_{as})$, $\nu(-COO^-_{s})$, ν(C=O) and ν(C–O) bands. A primary reason is that the morphology and size of TiO_2 nanocrystals can affect the energy level binding mode between the N719 and the TiO_2. Therefore, the vibration bands of carboxylic acid and carboxylate groups used in grafting the N719 onto TiO_2 nanocrystals with different morphology and size reveal the obvious differences. Besides, ν(C–H) bands of tetrabutylammonium symmetric and asymmetric $-CH_2$ and $-CH_3$ groups of the N719 anchoring onto the TiO_2

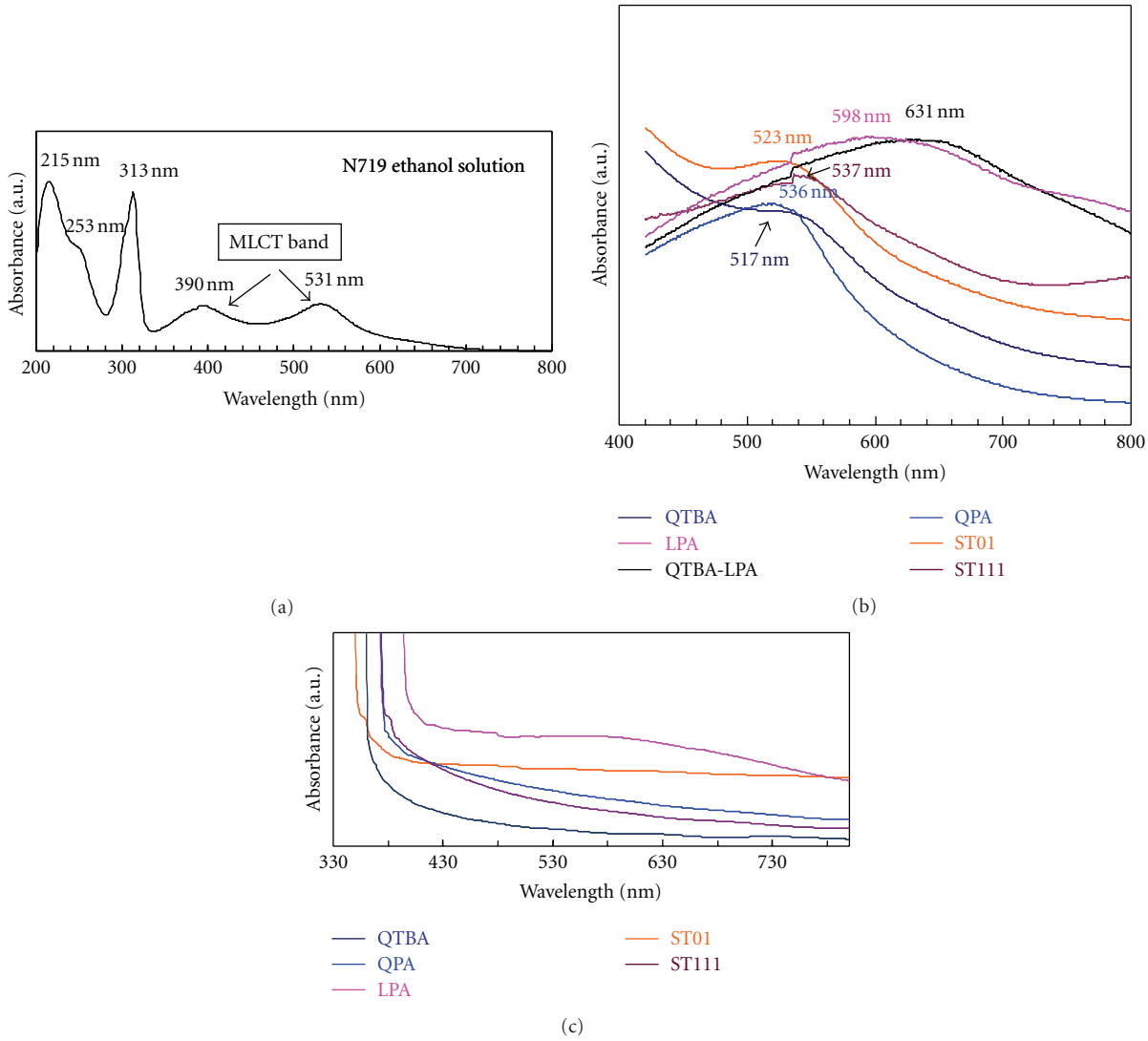

FIGURE 4: Absorption spectra of N719 dye in ethanol solution (a) and adsorbed onto TiO_2 nanocrystal films (b). Absorption spectra of the TiO_2 nanocrystals film samples (c).

surface also reveal larger differences with the change of the morphology and the size of TiO_2 nanocrystals due to steric reasons.

3.3. Photovoltaic Properties. Typical current-voltage characteristic curves (thin line) for ST01-based, ST111-based, QTBA-based, QPA-based, and LPA-based DSCs are presented in Figure 6. The power conversion efficiency (η) of the cell can be evaluated from the short circuit photocurrent density (J_{sc}), the open circuit potential (V_{oc}), the fill factor (ff) of the cell, and the intensity of the incident light ($I_s = 100\,mW/cm^2$) using the equation $\eta = J_{sc}\ V_{oc}\ ff/I_s$. Photovoltaic parameters of J_{sc}, V_{oc}, ff, and η for the DSCs prepared by using the above TiO_2 nanocrystals with different morphology and size are summarized in Table 2. These cell parameters are evaluated from the current-voltage curves of the DSCs in Figure 6.We observe that the V_{oc} value increases in the order of ST01 < QPA < QTBA < LPA, and the J_{sc} value increases in the order of LPA < ST01 < QPA < QTBA. It is also observed that QPA sample has the lowest ff and η values, and LPA sample has the highest ff and η values. The QTBA sample with the highest J_{sc} value has lower η value due to the lower ff value. One of the important factors is the conductivity of the TiO_2 film. It has been reported that increasing the conductivity of TiO_2 film by adding one-dimensional nanowire-like particles into the spherical nanoparticles can enhance the ff value [23, 24].

In order to improve the performance of the DSCs prepared by single TiO_2 nanocrystals samples, QTBA, QPA, and ST01 samples (80%) were mixed with the long leaflike LPA(20%), respectively. The photocurrent-voltage characteristic curves (thick line) of DSCs prepared respectively using the QTBA-LPA, QPA-LPA, and ST01-LPA mixed samples are shown in Figure 6. The cell parameters of V_{oc}, J_{sc}, ff, and η for corresponding DSCs are summarized in Table 2. The cell parameters of V_{oc}, J_{sc}, ff, and η for the DSC

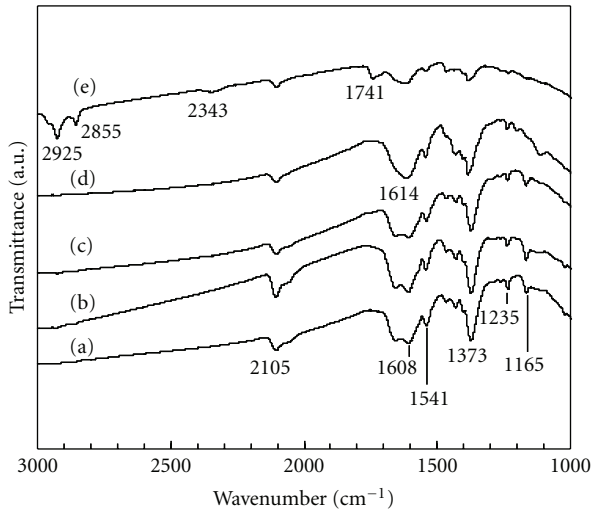

Figure 5: FT-IR spectra of the TiO_2 nanocrystals samples adsorbed by N719 dye. (a) N719-ST01; (b) N719-ST111; (c) N719-QTBA; (d) N719-QPA; (e) N719-LPA.

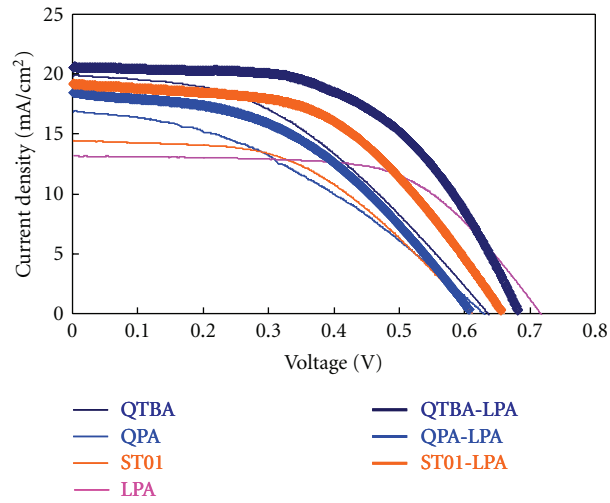

Figure 6: Current-Voltage characteristics for DSCs prepared using TiO_2 nanocrystals samples.

Table 2: Photovoltaic parameters of DSCs fabricated using the TiO_2 nanocrystals and thickness of the TiO_2 nanocrystals films.

Sample	V_{oc} (V)	J_{sc} (mA/cm^2)	ff	η (%)	Thickness (μm)
ST01	0.612	14.5	0.49	4.36	10.3
QTBA	0.637	19.9	0.43	5.40	5.8
QPA	0.630	16.9	0.38	4.07	10.6
LPA	0.717	13.2	0.61	5.77	8.8
ST01-LPA	0.659	19.2	0.51	6.45	19.6
QTBA-LPA	0.685	20.6	0.55	7.74	7.8
QPA-LPA	0.612	18.5	0.45	5.11	10.1

enhance 8%, 4%, 28%, and 43%, respectively, comparing with that for original QTBA-based DSC. And the η value (7.74%) is also much higher than that of P25-based DSC (6.3%) [25]. The η and J_{sc} values of the DSCs enhance 26% and 9% for QPA-LPA, and 48% and 32% for ST01-LPA, respectively, comparing with that for corresponding original DSC. The results reveal that the performance of the DSCs is significantly improved. The main reasons enhanced cell parameters are that the addition of the one-dimensional leaflike particles can effectively increase the conductivity for transferring the photoelectrons from the TiO_2 film to FTO glass surface that decreases the recombination loss of injected electrons in TiO_2 film [26], and the relatively larger particle size of LPA also causes the light-trapping effect that enhances the J_{sc} [27]. The other reason of the improved cell parameters is that the added LPA with the long leaf-like morphology and larger size brings the larger red shifts of MLCT band of the N719 dye onto the TiO_2 nanocrystals films. The J_{sc} value (mA/cm^2) increases from 19.9 for QTBA to 20.6 for QTBA-LPA with the red shift of λ_{max} of the MLCT band from 517 to 631 nm. This red shift can expand the absorption region of visible light and thus increases the utilization rate to visible light. Therefore, this would enhance J_{sc} and η values of the DSCs as well.

4. Conclusions

The morphology and the size of TiO_2 nanocrystals can affect on the UV-vis and FT-IR spectra of the sensitizer anchored on their surfaces. In particular, the low-energy metal-to-ligand charge-transfer transitions band in the visible absorption spectra is shifted after dye N719 adsorbed onto TiO_2 nanocrystals. The maximum wavelength of low-energy MLCT bands increases in the order of quadrate < spherical < long crystal. The wavelength increases with the particle size as well. The results indicate that there is a red shift of MLCT band in the spectra obtained by using TiO_2 nanocrystals with long morphology and large size compared to that of N719 in solution. And a larger red shift of the MLCT band arises after TiO_2 nanocrystals with small size mixed with some long nanocrystals, which increases the utilization rate to visible light. This is a reason that the DSC prepared by using such film has better performance than that of before mixing. The morphology and the size of TiO_2 nanocrystals affect strongly on the $\nu(-COO^-_{as})$, $\nu(-COO^-_{s})$, ν(C=O), and ν(C–O) bands. The main reason is that the morphology and the size of TiO_2 nanocrystals can affect the energy level binding mode between the N719 and the TiO_2. Therefore, the vibration bands of carboxylic acid and carboxylate groups used in grafting the N719 onto TiO_2 nanocrystals with different morphology and size reveal the obvious differences.

Acknowledgments

This work was supported by the Natural Science Foundation of China (no. 21173003), the Scientific Research Project from Science and Technology Department of Shaanxi Province (no. 2011JM2009), and the Key Research Project from Baoji University of Arts and Sciences (no. ZK1051).

References

[1] B. O'Regan and M. Grätzel, "A low-cost, high-efficiency solar cell based on dye-sensitized colloidal TiO_2 films," *Nature*, vol. 353, no. 6346, pp. 737–740, 1991.

[2] K. Sayama, H. Sugihara, and H. Arakawa, "Photoelectrochemical properties of a porous Nb_2O_5 electrode sensitized by a ruthenium dye," *Chemistry of Materials*, vol. 10, no. 12, pp. 3825–3832, 1998.

[3] S. Nakade, M. Matsuda, S. Kambe et al., "Dependence of TiO_2 nanoparticle preparation methods and annealing temperature on the efficiency of dye-sensitized solar cells," *Journal of Physical Chemistry B*, vol. 106, no. 39, pp. 10004–10010, 2002.

[4] M. K. Nazeeruddin, F. De Angelis, S. Fantacci et al., "Combined experimental and DFT-TDDFT computational study of photoelectrochemical cell ruthenium sensitizers," *Journal of the American Chemical Society*, vol. 127, no. 48, pp. 16835–16847, 2005.

[5] Y. Chiba, A. Islam, Y. Watanabe, R. Komiya, N. Koide, and L. Han, "Dye-sensitized solar cells with conversion efficiency of 11.1%," *Japanese Journal of Applied Physics*, vol. 45, no. 24–28, pp. L638–L640, 2006.

[6] P. Wen, Z. Tao, Y. Ishikawa, H. Itoh, and Q. Feng, "Dye-sensitized solar cells based on anatase TiO_2 nanocrystals exposing a specific lattice plane on the surface," *Applied Physics Letters*, vol. 97, no. 13, Article ID 131906, 2010.

[7] F. Gao, Y. Wang, D. Shi et al., "Enhance the optical absorptivity of nanocrystalline TiO_2 film with high molar extinction coefficient ruthenium sensitizers for high performance dye-sensitized solar cells," *Journal of the American Chemical Society*, vol. 130, no. 32, pp. 10720–10728, 2008.

[8] S. K. Deb, "Dye-sensitized TiO_2 thin-film solar cell research at the national renewable energy laboratory (NREL)," *Solar Energy Materials and Solar Cells*, vol. 88, no. 1, pp. 1–10, 2005.

[9] M. Murayama, N. Nishikawa, E. Yamazaki, M. Shoyama, N. Hashimoto, and K. Masuyama, "Nano-porous TiO_2 thin film for dye-sensitized solar cell," *Transactions of the Materials Research Society of Japan*, vol. 29, no. 4, pp. 1451–1454, 2004.

[10] T. Horiuchi, H. Miura, K. Sumioka, and S. Uchida, "High efficiency of dye-sensitized solar cells based on metal-free indoline dyes," *Journal of the American Chemical Society*, vol. 126, no. 39, pp. 12218–12219, 2004.

[11] H. Qin, S. Wenger, M. Xu et al., "An organic sensitizer with a fused dithienothiophene unit for efficient and stable dye-sensitized solar cells," *Journal of the American Chemical Society*, vol. 130, no. 29, pp. 9202–9203, 2008.

[12] J. Song, F. Zhang, C. Li et al., "Phenylethyne-bridged dyes for dye-sensitized solar cells," *Journal of Physical Chemistry C*, vol. 113, no. 30, pp. 13391–13397, 2009.

[13] P. Wang, S. M. Zakeeruddin, J. E. Moser, R. Humphry-Baker, and M. Grätzel, "A solvent-free, $SeCN^-/(SeCN)_3^-$ based ionic liquid electrolyte for high-efficiency dye-sensitized nanocrystalline solar cells," *Journal of the American Chemical Society*, vol. 126, no. 23, pp. 7164–7165, 2004.

[14] A. Hauch and A. Georg, "Diffusion in the electrolyte and charge-transfer reaction at the platinum electrode in dye-sensitized solar cells," *Electrochimica Acta*, vol. 46, no. 22, pp. 3457–3466, 2001.

[15] M. Dürr, A. Yasuda, and G. Nelles, "On the origin of increased open circuit voltage of dye-sensitized solar cells using 4-ferf-butyl pyridine as additive to the electrolyte," *Applied Physics Letters*, vol. 89, no. 6, Article ID 061110, 2006.

[16] H. Kusama, M. Kurashige, and H. Arakawa, "Influence of nitrogen-containing heterocyclic additives in I^-/I_3^- redox electrolytic solution on the performance of Ru-dye-sensitized nanocrystalline TiO_2 solar cell," *Journal of Photochemistry and Photobiology A*, vol. 169, no. 2, pp. 169–176, 2005.

[17] H. Kusama and H. Arakawa, "Influence of pyrazole derivatives in I^-/I_3^- redox electrolyte solution on Ru(II)-dye-sensitized TiO_2 solar cell performance," *Solar Energy Materials and Solar Cells*, vol. 85, no. 3, pp. 333–344, 2005.

[18] M. K. Nazeeruddin, R. Humphry-Baker, P. Liska, and M. Grätzel, "Investigation of sensitizer adsorption and the influence of protons on current and voltage of a dye-sensitized nanocrystalline TiO_2 solar cell," *Journal of Physical Chemistry B*, vol. 107, no. 34, pp. 8981–8987, 2003.

[19] P. Wen, H. Itoh, W. Tang, and Q. Feng, "Single nanocrystals of anatase-type TiO_2 prepared from layered titanate nanosheets: formation mechanism and characterization of surface properties," *Langmuir*, vol. 23, no. 23, pp. 11782–11790, 2007.

[20] P. Wen, H. Itoh, W. Tang, and Q. Feng, "Transformation of layered titanate nanosheets into nanostructured porous titanium dioxide in polycation solution," *Microporous and Mesoporous Materials*, vol. 116, no. 1–3, pp. 147–156, 2008.

[21] P. Wen, Y. Ishikawa, H. Itoh, and Q. Feng, "Topotactic transformation reaction from layered titanate nanosheets into anatase nanocrystals," *Journal of Physical Chemistry C*, vol. 113, no. 47, pp. 20275–20280, 2009.

[22] K. S. Finnie, J. R. Bartlett, and J. L. Woolfrey, "Vibrational spectroscopic study of the coordination of (2,2′-bipyridyl-4,4′dicarboxylic acid)ruthenium(II) complexes to the surface of nanocrystalline titania," *Langmuir*, vol. 14, no. 10, pp. 2744–2749, 1998.

[23] S.-H. Kang, S.-H. Choi, M.-S. Kang et al., "Nanorod-based dye-sensitized solar cells with improved charge collection efficiency," *Advanced Materials*, vol. 20, no. 1, pp. 54–58, 2008.

[24] Y.-B. Tang, C.-S. Lee, J. Xu et al., "Incorporation of graphenes in nanostructured TiO_2 films via molecular grafting for dye-sensitized solar cell application," *ACS Nano*, vol. 4, no. 6, pp. 3482–3488, 2010.

[25] P. Wen, M. Xue, Y. Ishikawa, H. Itoh, and Q. Feng, "Relationships between cell parameters of dye-sensitized solar cells and dye-adsorption parameters," *ACS Applied Materials & Interfaces*, vol. 4, no. 4, pp. 1928–1934, 2012.

[26] A. Usami, "Theoretical simulations of optical confinement in dye-sensitized nanocrystalline solar cells," *Solar Energy Materials and Solar Cells*, vol. 64, no. 1, pp. 73–83, 2000.

[27] Y. Tachibana, K. Hara, K. Sayama, and H. Arakawa, "Quantitative analysis of light-harvesting efficiency and electron-transfer yield in ruthenium-dye-sensitized nanocrystalline TiO_2 solar cells," *Chemistry of Materials*, vol. 14, no. 6, pp. 2527–2535, 2002.

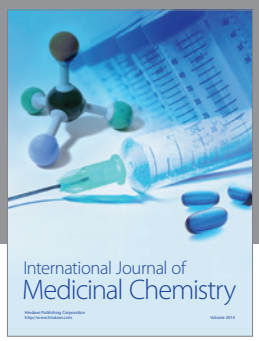

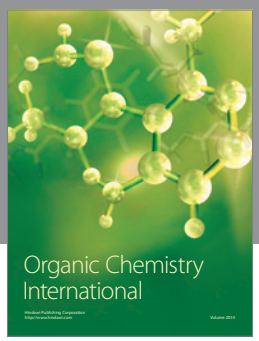

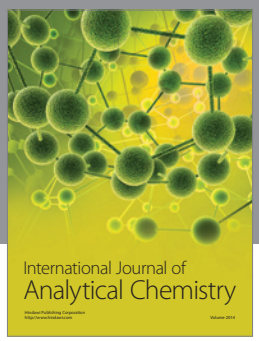

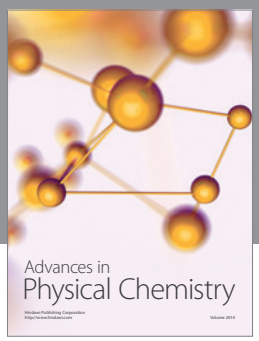

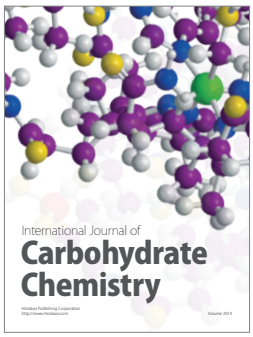

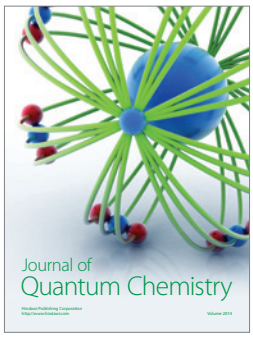

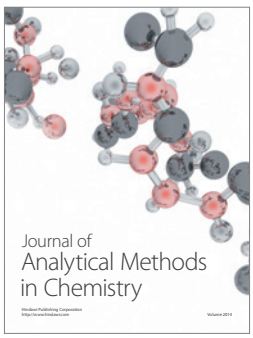

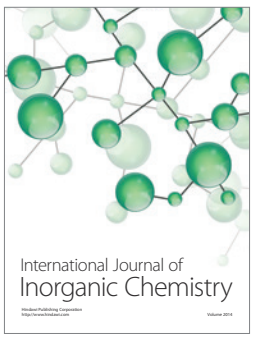

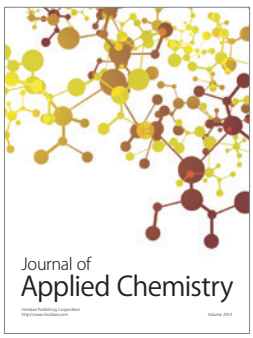

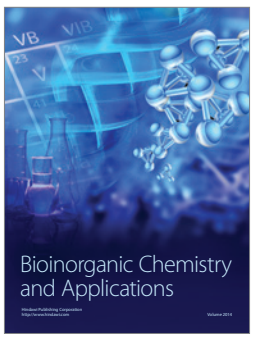

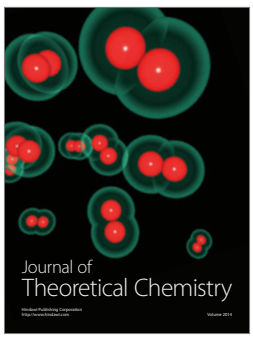

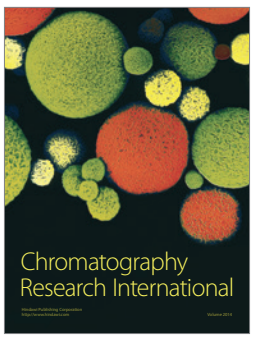

Hindawi

Submit your manuscripts at
http://www.hindawi.com